

Molecular Dynamics Simulation Study of Chlorophyll a in Different Organic Solvents

Khadga Karki and Danilo Roccatano*

School of Engineering and Science, Jacobs University Bremen, Campus Ring 1, D-28759, Bremen, Germany

 Supporting Information

ABSTRACT: Herein, we present a new model of chlorophyll a for molecular dynamics simulations based on the optimized potentials for liquid simulations force field. The new model was used to study the structural and dynamic properties of the molecule in three different solvents: water, methanol, and benzene. The results of the simulations show that structural and dynamic properties of the chlorin ring are similar in both methanol and benzene. In methanol and water, the magnesium in the chlorin ring binds the oxygen of the solvent molecules with residence times of 2566 and 1300 ps, respectively. In both methanol and benzene, the phytol tail shows a worm-like chain distribution with a larger persistence length for the molecule in benzene. On the contrary, chlorophyll a in water adopts a more compact structure with the phytol chain folded onto the chlorin ring. This conformation is consistent with the expected conformation of the aggregates of chlorophyll a in aqueous environments. Finally, the rotational time constants obtained with our model from the simulations in methanol (125 ps) and benzene (192 ps) are in good agreement with the value extrapolated from the experimental data.

■ INTRODUCTION

Chlorophylls are among the most important molecules in nature.¹ Chlorophyll a (Chl A), one of the chlorophyll molecules, plays a key role in the light-harvesting complex (LHC), by collecting and funneling light, and as an electron carrier in the photosynthetic reaction centers, by separating charges and transferring electrons across the photosynthetic membrane.^{2,3} These marvelous biological processes are the result of cooperative effects, depending crucially not only on the electronic properties of an individual Chl A molecule but also on the way they are assembled.⁴ The structural organization of the chlorophyll molecules in photosynthetic systems is orchestrated by electrostatic and van der Waals and other nuanced interactions of different functional groups with the surrounding environment. The phytol tail of Chl A is hydrophobic, while the magnesium (Mg), being coordinatively unsaturated, attracts nucleophilic polar molecules. In nonpolar solvents, like benzene, the coordination of Mg is saturated by the electron donor C=O group of another Chl A molecule leading to the formation of dimers and aggregates. In polar solvents, like methanol, the nucleophilic solvent molecules compete with the C=O group for the coordination with the Mg thereby preventing aggregation. However, in other polar solvents, like water, they form large aggregates² because of the intermolecular hydrogen bonding or smaller aggregates, like in mixture of acetonitrile/water, because of the hydrophobic effects of the phytol tail.⁵

Most of the experimental techniques employed to understand these interactions (for example see the references)^{6–11} do not provide the information with atomic resolution. Therefore, use of theoretical/computational model can complement these data and provides useful insights for interpretation and comprehension of the interactions. Several computational studies, based on molecular dynamics (MD) simulations and quantum mechanics (QM) methods, on the structural and spectroscopic properties of chlorophylls are available in literature.¹² MD simulation studies

of chlorophylls, including the ones embedded in the LHCs (see for example refs 13–16), have also been reported. However, to the best of our knowledge, none of these models have been optimized and tested against the properties of isolated molecules in different solvents. In this first paper, we use a new model of Chl A based on the optimized potentials for liquid simulations (OPLS) force field to study the structural and dynamic properties of Chl A in three different solvents: water, methanol, and benzene. We have considered methanol (dielectric constant $\epsilon = 33$) and benzene ($\epsilon = 2.28$) because both of them dissolve Chl A, and hence, it is interesting to analyze their effect on the conformation of the molecule in the different environments. On the contrary, simulations in water can be used to test the force field and to get insights into the mechanism of water-mediated aggregation. In the paper, we have focused mainly on investigating the interaction of Chl A with the solvent molecules by comparing our results with the experimental data¹⁷ and recently published QM calculations.¹⁸

The paper is organized as follows. The modeling of the Chl A force field is presented in the Material and Methods Section. The structural and dynamic properties of the molecule are presented in the Results and Discussion Section. In this part, we also report a preliminary study on the aggregation of Chl A. Finally, in the Conclusion Section, a summary of the study with an outlook on the further applications of the model is presented.

■ MATERIAL AND METHODS

QM Calculations. Chlorophyllide a molecule was used instead of Chl A to calculate the binding energy of water and methanol to the Mg. The starting structure of chlorophyllide a with a water molecule coordinated to the Mg was obtained from the crystal

Received: August 18, 2010

Published: February 24, 2011

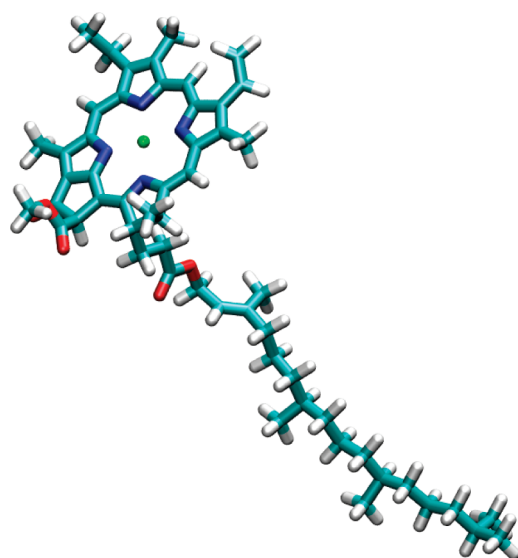


Figure 1. Optimized geometry of Chlorophyll a in vacuum.

structure of the ethyl derivative of the molecule.¹⁹ The molecule was isolated from water, and the ethyl group was substituted by a hydrogen to retain the chlorophyllide a structure. Geometry optimization was done with B3LYP method and 6-31G** basis set in implicit solvation condition using the integral-equation-formalism protocol²⁰ formulation of the polarizable continuum model (PCM).²¹ A water molecule was placed 0.3 nm above the Mg of the optimized chlorophyllide, and the geometry of the complex was optimized again using the same procedure, after which counterpoise correction was used to calculate the binding energy of the water molecule to the Mg. Normal mode analysis was done on the water and the chlorophyllide molecules separately to estimate the thermal corrections used to calculate the Helmholtz free energy. Similar calculations were done in the case of methanol and benzene. The optimized geometries used in the QM calculations are given in the Supporting Information.

QM calculations were also done on Chl A taken from the crystal structure of the LHC of spinach²² (pdb code: 1RWT) to obtain the optimized structure (shown in Figure 1) and the partial charges of the molecule. Geometry optimization was done using the restricted B3LYP method with the 6-31G* basis set, and the atomic charges were calculated by fitting the molecular electrostatic potential of the electronic density using the CHELPG procedure.²³ The coordinates of the optimized structure and the corresponding partial charges are reported in Table 1 and 2 of the Supporting Information.

All the QM calculations were performed using the program Gaussian 09.²⁴

Chl A Force Field Parameters. We used the OPLS-AA^{25–28} force field with additional parameters for partial charges, bond lengths, angles, and dihedral angles based upon our QM calculations. The force constants for the bond angles and the torsional interactions and the Lennard-Jones parameters were adapted from the OPLS parameters, while the partial charges were taken from the QM calculations described above. The full set of parameters are reported in the Supporting Information. OPLS force field-based models were also used for methanol,²⁵ water (TIP4P model),²⁹ and benzene.³⁰

MD Simulations. All MD simulations and analysis were performed using the GROMACS package (version 4.0.7).³¹

The geometry optimized Chl A molecule was immersed in three boxes containing the three different solvents. The simulations in water were done in a 5.34 nm long cubic box containing 4999 water molecules coupled to an external bath at 300 K using the Nose-Hoover³² thermostat and to a barostat at 1 bar using the Parrinello-Rahman^{33,34} isotropic pressure coupling method, as implemented in GROMACS. The coupling time constants for the control of the temperature (τ_T) and the pressure (τ_P) were set to 0.2 and 1.0 ps, respectively, and the compressibility was set to 4.5×10^{-5} bar⁻¹. For the simulations in methanol, a cubic box of length 4.9 nm containing 1685 molecules was used. The coupling time constants τ_T and τ_P were set to 0.1 and 1.5 ps, respectively, and the compressibility was set to 1.2×10^{-4} bar⁻¹. For the simulations in benzene, a cubic box of length 6.31 nm containing 1685 solvent molecules was used. The coupling time constants τ_T and τ_P were set to 0.2 and 2.5 ps, respectively, and the compressibility was set to 9.5×10^{-5} bar⁻¹. All the solvent molecules within 0.15 nm of any Chl A atom were removed, and the systems were energy minimized with the steepest-descent method for 5000 steps. The bond lengths were constrained using the SETTLE algorithm³⁵ for the water molecules and the LINCS algorithm³⁶ for the other molecules. A 1.0–1.2 nm switched cutoff radius was used for the Lennard-Jones interactions. The PME method³⁷ was used for the electrostatic interactions with PME order of 4, Fourier spacing of 0.12 nm, and dielectric permittivity of 1. The short-range neighbor list was set to 1.4 nm. All the atoms were given an initial velocity obtained from a Maxwellian distribution at 300 K. A time step of 2 fs was used in the simulations, and they were equilibrated by 500 ps of MD runs to allow the relaxation of the solvent molecules. After the equilibration, 50 ns production run was performed for each simulation. Simulations were also performed at constant temperature and volume (NVT) conditions to calculate the potential of mean force (PMF)³⁸ of the interaction of the solvent molecules with the Mg. Simulations of systems with 10 Chl A molecules in the three solvents were also performed to test the formation of aggregates in the different solvents. The boxes used in the simulations contained 10 889, 10 828, and 10 827 molecules of water, methanol, and benzene, respectively.

Cluster Analysis of the Chl A Conformation. A reliable estimation of the conformational space explored by the simulations is the evaluation of the number of different configurations generated during the trajectory.³⁹ The cluster analysis of trajectories was performed using the method proposed by Daura et al.⁴⁰ on a total of 5000 structures sampled every 10 ps. The clustering algorithm was applied to the heavy atoms of Chl A. The criteria of similarity for two structures was a positional root-mean-square deviation with the cutoff set to 0.3 nm. Similar analysis was done to the chlorin ring using the cutoff of 0.02 nm.

Phytol Tail analysis. The conformational dynamics of the phytol chain was analyzed by calculating the distribution of the beginning-to-end chain length. In the case of methanol and benzene, the distribution was compared with the worm-like chain (WLC)^{41,42} model given by

$$P(R) = \frac{4\pi NR^2}{l_c^2 A^{9/2}} \exp\left(-\frac{3l_c}{4l_p A}\right) \quad (1)$$

where R is the coordinate along the contour of the tail, N is the normalization factor, l_p is the persistence length, l_c is the contour

length and A is given by

$$A = 1 - \frac{R^2}{l_c^2} \quad (2)$$

Translational and Rotational Diffusion. The diffusion coefficient of Chl A was calculated using the Einstein relation:⁴³

$$6Dt = \lim_{t \rightarrow \infty} \langle |\mathbf{r}_i(t) - \mathbf{r}_i(0)|^2 \rangle \quad (3)$$

where $\mathbf{r}_i(t)$ is the coordinate vector of the particle i at time t , and $\mathbf{r}_i(0)$ the coordinate vector of the particle i at time $t = 0$.

Besides the translational diffusion, rotational diffusion provides useful information on how a solute interacts with the solvents. The rotational diffusion of the chlorin ring was calculated using the autocorrelation function of the vector normal to the plane of the ring:

$$C_2(t) = \langle P_2(\mathbf{n}(0) \cdot \mathbf{n}(t)) \rangle \quad (4)$$

where P_2 is the Legendre polynomial of the order 2, \mathbf{n} is the unit vector pointing out of the plane of the ring, and the brackets indicate the average along the trajectory.⁴⁴ The plane of the ring was determined using the atoms that show the least fluctuations in the ring.

Rotational Relaxation Time Constants. The correlation function measured in the experiments is usually approximated by⁴⁵

$$C_2(t) = a \exp[-(6D_r t)] = a \exp(-t/\tau_2) \quad (5)$$

and τ_2 is the rotational relaxation time. Thus, the relaxation time obtained from the simulations is related to the rotational diffusion coefficient by

$$\tau_2 = \frac{1}{6D_r} \quad (6)$$

Viscosity of the Solvents. To compare the rotational relaxation time constants obtained from the simulations with the experimentally determined time constants, the viscosity of the solvents used in the simulations and the experiments has to be taken into account. The viscosities of the solvents used in the simulations were computed from the nonequilibrium MD simulations.⁴⁶

In this method, a sinusoidally varying acceleration, with the profile given by

$$a_x(z) = A \cos(2\pi z/l_z) \quad (7)$$

where A is the amplitude of the acceleration and l_z is the height of the box, was applied in the x direction. In these simulations the length of the boxes in z -direction were set three times longer than in the other directions. The generated velocity profile due to the acceleration can be written as

$$v_x(z) = V \cos(2\pi z/l_z) \quad (8)$$

where V is the amplitude of the generated velocity. The viscosity was then calculated using the relation:

$$\eta = \frac{A}{V} \rho (l_z / 2\pi)^2 \quad (9)$$

where ρ is the density of the solvent.

Different simulations were done varying the amplitude of the acceleration. The viscosity at the equilibrium was determined by interpolation.

Solvation Geometry and Energetics. The distribution of solvent molecules around the Mg plays an important role in solvation and solvent-mediated aggregation of Chl A molecules. The pair correlation function, $g_{x,y}(r)$, and the spatial distribution function (SDF)⁴⁷ were used to get insight into the local ordering of the solvent molecules. The subscripts x and y in $g_{x,y}(r)$ denote the particle types, and r denotes the radial distance between the particles x and y . The number of solvent molecules in the different solvation shells of the Mg was calculated using the running integration number (RIN):

$$n = 4\pi\rho_0 \int_0^R g_{Mg,X}(r) r^2 dr \quad (10)$$

where X denotes either O (oxygen atom) or C (carbon atom), and ρ_0 is the number density of the solvent molecule of which the RIN is calculated.

The anisotropic distribution of the solvent atoms around the chlorin ring was analyzed using the SDFs calculated in the Cartesian coordinate system with the origin of the system fixed to the Mg, two of the vectors defined by the vectors joining Mg to the nitrogen atoms and a third vector orthogonal to the plane defined by the first two vectors.

The PMFs of the interaction of the solvent molecules with the Mg, as a function of radial distance, were calculated from the pair correlation functions obtained from the NVT simulations using the relation:³⁸

$$g_{Mg,X}(r) = \exp\left(-\frac{w(r)}{kT}\right) \quad (11)$$

where $w(r)$ is the PMF, k is the Boltzmann constant, and T is the temperature.

Residence Time of Water and Methanol. The lifetime of the contact between the Mg and the solvent molecules in a given solvation shell provides important information about the solvation dynamics. This information can be obtained from MD trajectories in different manners.⁴⁴ A common approach is the use of the so-called survival time correlation function:⁴⁸

$$P_\alpha(t) = \sum_{j=1}^N \sum_{t'} P_{\alpha,j}(t', t' + t) \quad (12)$$

where the probability function, $P_{\alpha,j}(t', t' + t)$ is a binary function that adopts a value of 1 if the solvent molecule labeled j has been in the referred solvation shell around site a from time t' to time $t + t'$, without escaping in this time interval (or leaving the shell during this interval for a time not longer than a t^* interval), and 0 otherwise. The value of $P_{\alpha,j}(t, t + t')$ is averaged over time and over all solvent molecules from conformations sampled from the MD simulation. $P_{\alpha,j}(t = 0)$ equals the average number of solvent molecules belonging to the solvation shell of the site j (i.e., the coordination number), and $P_{\alpha,j}(t)$ gives the average number of solvent molecules that still remain in the hydration shell after a time t from when they first entered the shell. The relaxation trend of $P_{\alpha,j}(t)$ provides information about the local dynamics of the solvation molecules. The value of $P_{\alpha,j}(t)$ can be approximated to an exponential function:⁴⁸

$$C_\alpha(t) = A \exp(-t/\tau) \quad (13)$$

where τ is the residence time.

■ RESULTS AND DISCUSSION

Structural Properties. The cluster analysis of the chlorin ring done with cutoff of 0.02 nm gave 11, 10, and 9 clusters from 5000 sampled structures in water, methanol, and benzene, respectively. The cumulative number of the clusters (Figure 2a) reaches a plateau indicating a good sampling of the conformational space. The first three clusters account for 99% (80, 10, and 9%), 99% (79, 11, and 9%), and 99% (80, 14, and 5%) of the structures in the three solvents, respectively. The representative structures of the first three clusters are shown in Figure 3. The average structure of the ring is planar. The deviations from the planarity involve different collective motions of the atoms in the ring. The root-mean-square fluctuations of the atoms (Figure 4) show that

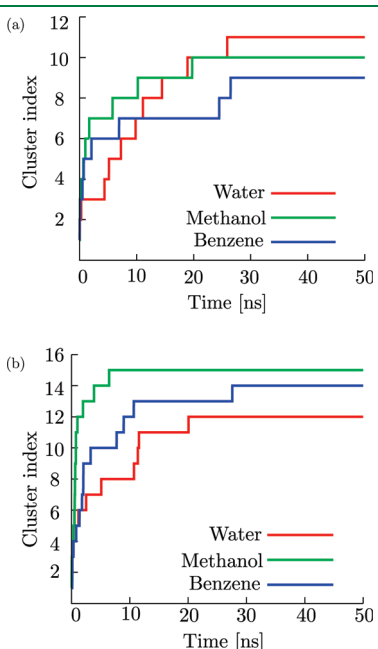


Figure 2. Cumulative distribution of the number of clusters obtained from the water, methanol, and benzene simulations: (a) chlorin ring and (b) all heavy atoms of Chl A.

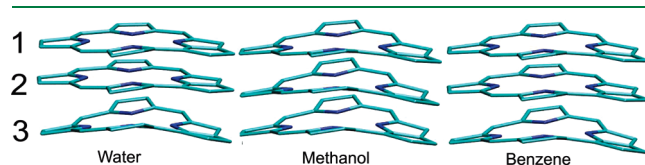


Figure 3. Representative configurations of the three most populated clusters of the chlorin ring.

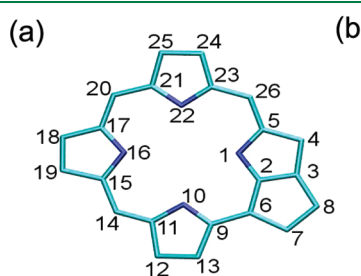


Figure 4. Root-mean-square fluctuations of the atoms of the chlorin ring (b). The numbering of the atoms is shown in (a).

atoms on the border of the chlorin ring have larger fluctuations than the atoms that connect the aromatic rings or the atoms in the inner part of the rings. Though the pattern of fluctuations in all the three solvents is similar, larger fluctuations are observed in water than in methanol or benzene due to the phytol tail which folds back onto the chlorin ring.

The cluster analysis of the complete molecule performed using a larger cutoff of 0.3 nm gave 12, 15, and 14 clusters from 5000 structures sampled from the simulations in water, methanol, and benzene, respectively. The cumulative number of the clusters (Figure 2b) reaches a plateau indicating a good sampling of the conformational space. The first three clusters account for 94, 71, and 75% of the total sampled structures in water, methanol, and benzene, respectively. The large variety of conformations is mainly determined by the hydrophobic phytol chain. The smaller number of clusters observed in the simulation in water is due to the folded configuration of the tail, which reduces its mobility. On the contrary, in methanol and benzene, the flexibility of the tail resembles that of a freely floating chain thereby increasing the number of conformations. In Figure 5 the beginning-to-end distribution of the phytol chain is reported. In methanol and benzene, the distributions are similar, spanning from 0.36 to 2.33 nm, with the main peak in methanol at 1.57 nm and in benzene at 1.76 nm. The WCL (eq 1) model fitted to the distributions gives contour and persistence lengths of $l_c = 2.47 \pm 0.02$ nm, $l_p = 0.239 \pm 0.006$ nm, and $l_c = 2.575 \pm 0.009$ nm, $l_p = 0.266 \pm 0.003$ nm in methanol and benzene, respectively. The comparison of the persistence lengths indicates that the chain in benzene is stiffer than in methanol. The distribution in water, which does not fit to the WLC model, is bimodal with the first peak at 0.57 nm corresponding to the tail folded onto the ring and the second peak at 1.4 nm corresponding to a more extended configuration.

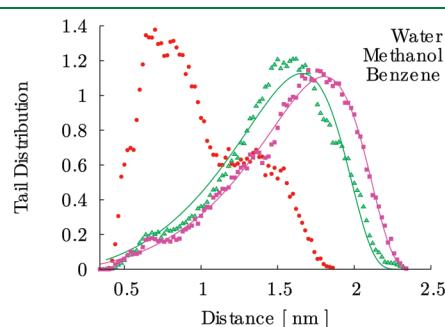
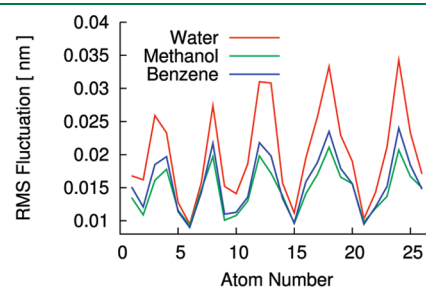


Figure 5. The distribution of the beginning-to-end distance of the phytol chain of Chl A in water, methanol, and benzene. The symbols indicate the data obtained from the simulations. The distribution in benzene and methanol is fitted to the worm-like chain model distribution (solid lines).



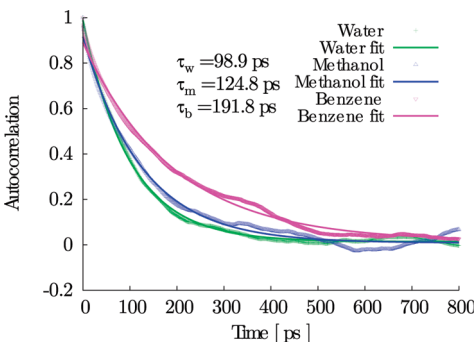


Figure 6. Correlation functions using second-order Legendre polynomial for the rotational diffusion of Chl A in water, methanol, and benzene. The correlation functions are fitted with exponential decay curves. The time constants for the decay, τ , are reported in the figure.

Linear and Rotational Diffusion. The rotational diffusion of a molecule in solution can be measured in real time using pump–probe techniques with ultrashort laser pulses. In these experiments, a pump pulse is used to select molecules with a defined orientation, in some cases the molecules can also be aligned with the laser pulses, and the probe pulse is used to interrogate the transient anisotropy in the system induced by the pump pulse. Rotational diffusion makes the system isotropic thereby diminishing the signal from the induced anisotropy. Few of these experiments have been done to measure the rotational dynamics of chlorophyll molecules. In one of the transient grating studies done on zinc methyl 13-desoxopyropheophorbide (Zn DMPPH), an analogous molecule, the measured relaxation time of the rotation of the molecule dissolved in tetrahydrofuran (THF) was 114 ps.⁴⁹ The relaxation time of the rotational dynamics of a molecule is directly proportional to the viscosity, η , of the solvent. Thus, to compare the experimental result with the results from simulations, the viscosities of the different solvents need to be taken into account. The experimental viscosity of THF is $\eta_T = 4.8 \times 10^{-4} \text{ Pa.s}$. The viscosities of the solvent models used in the simulations, determined by nonequilibrium MD simulations,⁵⁰ are $\eta_w = (5.6 \pm 0.7) \times 10^{-4} \text{ Pa.s}$, $\eta_m = (5.4 \pm 0.7) \times 10^{-4} \text{ Pa.s}$, and $\eta_b = (7.4 \pm 0.9) \times 10^{-4} \text{ Pa.s}$ for water, methanol, and benzene, respectively.

In the approximation that the geometry of the molecule is unchanged in different solvents, the viscosities and the rotational time constants τ follow the relation:

$$\frac{\tau_x}{\tau_y} = \frac{\eta_x}{\eta_y} \quad (14)$$

where subscripts x and y represent two different solvents. The expected rotational time constant of Zn DMPPH in water, methanol, and benzene models estimated using eq 14 are $\tau_{2,w} = 135 \pm 15$, $\tau_{2,m} = 128 \pm 14$, and $\tau_{2,b} = 176 \pm 30$ ps, respectively. Subscripts w, m, and b refer to the solvents water, methanol, and benzene, respectively. The time constants of the exponential functions used to fit the second-order correlation functions obtained from the simulations (Figure 6) are $\tau_w = 99$, $\tau_m = 125$, and $\tau_b = 192$ ps. The rotational diffusion time constants obtained from simulations in methanol and benzene are close to the respective estimated rotational time constants. In water, the time constant obtained from the simulation is slightly lower than the corresponding estimate from the experiment, which could be due to the influence of the solvent in the geometry of the

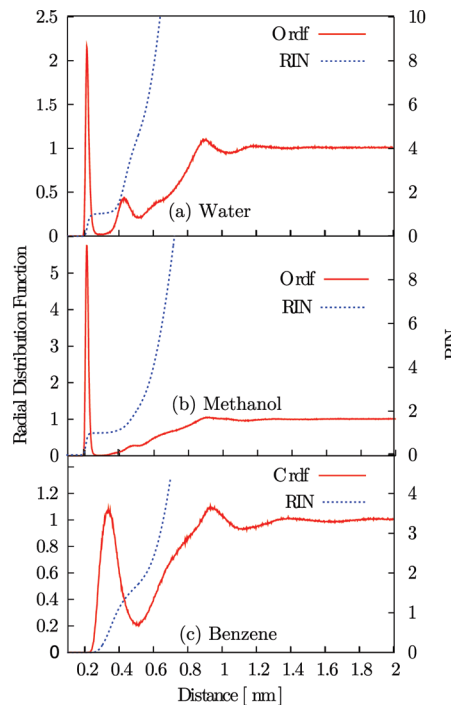


Figure 7. The radial distribution functions and the running integration numbers of the oxygen atoms of water and methanol and the carbon atoms of benzene around the Mg atom.

molecule. In water, as noted previously, the tail folds back to the chlorin ring, thereby decreasing the cross-section of the molecule as well as the moment of inertia and hence the faster rotational motion.

The rotational diffusion coefficients computed using eq 6 are 1.68, 1.33, and 0.87 rad²/ns in water, methanol, and benzene, respectively. To the best of our knowledge, direct experimental determination of rotational diffusion coefficients of Chl A or related molecules is not yet done. However, the values obtained from the simulations can be considered quite reliable, as the relaxation times obtained from the simulations are close to those estimated from the available experimental data.

Finally, the linear diffusion constants estimated using eq 3 are 0.47×10^{-5} , 0.52×10^{-5} , and $0.40 \times 10^{-5} \text{ cm}^2 \text{s}^{-1}$ in water, methanol, and benzene, respectively.

Chl A Solvation. The coordination unsaturation of the Mg can be satisfied by nucleophilic ligands.² The ligands can form both the Chl·L₁ and Chl·L₂ complexes, where Chl·L₁ is the complex formed with a ligand occupying one of the axial positions, while Chl·L₂ is the complex formed with two ligands occupying the axial positions on both the sides of the chlorin plane. The coordination of the methanol and water molecules to the Mg can be studied with the pair correlation function $g_{\text{Mg},\text{O}}$. In Figure 7, the $g_{\text{Mg},\text{O}}$ of both the solvents are shown. They have the first peak located at 0.21 nm. The narrow width of the peaks indicates that the oxygen atom is strongly bound to the Mg in both the solvents. The average number of oxygen atoms within the first solvation shell (up to 0.28 nm) is 1.02 and 1.01 for water and methanol, respectively (see Figure 7). This indicates that the Mg is predominantly penta-coordinated. The average number of oxygen atoms within the second solvation shell (up to 0.50 nm in water and 0.52 nm in methanol) is 4.33 and 2.19 in water and methanol, respectively.

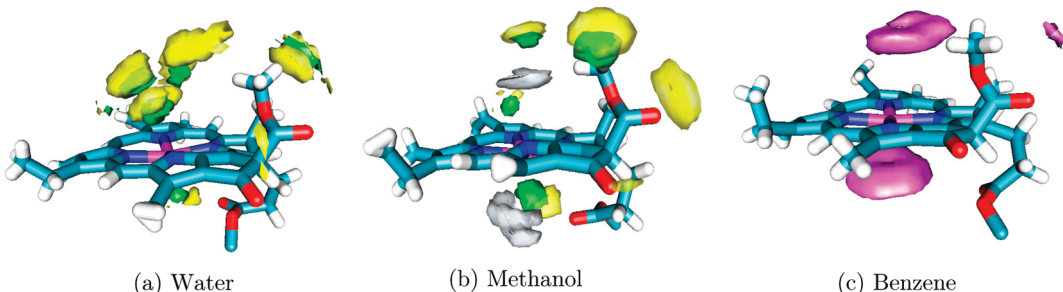


Figure 8. Spatial distribution function of oxygen and hydrogen atoms of water molecules (a), methanol molecules (b), and carbon atoms of benzene molecules (c) around the chlorin ring. Color coding for the contour surfaces: green for O, yellow for H in hydroxyl group, gray for H in methyl group, and magenta for C in the benzene. The contour values of the iso surfaces are 10 for both the hydrogens and oxygens in water; 22, 9, and 15 for methyl hydrogens, hydroxyl hydrogens, and oxygens, respectively, in methanol; and 12 for the carbons in benzene.

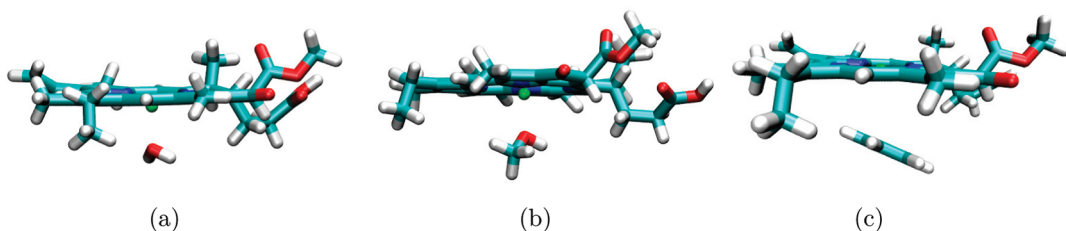


Figure 9. The optimized geometry of chlorophyllide–water (a), chlorophyllide–methanol (b), and chlorophyllide–benzene (c) complexes. The oxygen atom of water and methanol is bound to the Mg atom of the chlorin ring. The distance between the oxygen and the Mg is 0.21 nm (a and b). The distance of the Mg from the center of the benzene ring is 0.38 nm. The plane of the benzene ring is slightly tilted at an angle to the plane of the chlorin ring (c).

In Figure 8a and b, the SDF of oxygen and hydrogen atoms of water and methanol around the chlorin ring is shown. The average structures of the chlorin ring shown in the figures are slightly distorted with the Mg atom displaced out of the plane of the ring. The distortion is opposite to the side with the ester $\text{C}=\text{O}$ group. The distances between the Mg and the plane of the chlorin ring defined by atoms 1, 10, and 22 (Figure 4a) are 0.023 and 0.027 nm in water and methanol, respectively. The B3LYP/6-31G** optimized structures of water–chlorophyllide and methanol–chlorophyllide complexes (Figure 9a and b, respectively) also show distortion of the chlorin ring. The distances between the Mg atom and the plane of the chlorin ring, as defined previously, are 0.040 and 0.037 nm in the water–chlorophyllide and the methanol–chlorophyllide complexes, respectively. The displacement observed in the optimized geometry of water–chlorophyllide complex is similar to the displacement of 0.039 nm observed in the crystal structure of ethyl–chlorophyllide a dihydrate.¹⁹ The displacement observed in the MD simulations is less than the displacement observed in the chlorophyllide crystal structure and close to the range of displacement of 0.011–0.025 nm observed in the chlorophyll molecules of the spinach major LHC crystal structure (1RWT).

The SDF of the oxygen atoms of water (Figure 8a) shows two densities on the axial position on both the sides of the chlorin ring. In the same figure, the SDF of the hydrogen atoms of water shows that the hydrogens of the water molecules bound to the Mg point outward from the ring, which is consistent with the B3LYP/6-31G** optimized structure of water–chlorophyllide complex as shown in Figure 9a. The distance between Mg and oxygen in the optimized structure is 0.211 nm, which agrees with the position of the first peak of the $g_{\text{Mg},\text{O}}$ from the simulation. In addition, the Mg–O distances in both the QM-optimized geometry and the SDF are similar to the distance of 0.204 nm observed in the crystal structure of ethyl chlorophyllide a

dihydrate.¹⁹ The SDF of the oxygen atoms shows other two high-density regions above the first on the upper side of the ring. The arrangement of these two regions indicates presence of hydrogen bonds between the water molecules in the two regions and the water molecules coordinated to the Mg. Aggregation of chlorophylls in aqueous medium has been attributed to the hydrogen bonding between the Mg-bound water molecule of one chlorophyll and the keto $\text{C}=\text{O}$ group of another chlorophyll molecule.^{51,52} The presence of water molecules chained with hydrogen bonds to the Mg coordinated water molecule is supported by the crystal structure of ethyl chlorophyllide a·2H₂O, as proposed by Strouse et al.¹⁹ In this crystal structure, the Mg-coordinated water molecule is simultaneously hydrogen bonded to the keto $\text{C}=\text{O}$ group of another ethyl chlorophyllide a and to the oxygen of the second water molecule. The second water molecule is then hydrogen bonded to the ester $\text{C}=\text{O}$ of the first ethyl chlorophyllide and to the propionic ester $\text{C}=\text{O}$ of a third ethyl chlorophyllide (see the cited paper of Strouse et al.).¹⁹ Coordination of water molecule to the Mg also plays a central role in the proposed models of the photoactive chlorophyll special pair;⁵² the SDF of the water molecules around the chlorin ring obtained from our simulations is consistent with these hypotheses.

The SDF of the oxygen of methanol (Figure 8b) shows three regions of high density of oxygen atoms: two above and one below the chlorin ring. The high densities on the axis above and below the Mg are due to the oxygen atoms bound to the Mg; the other high density on the side of the density above the Mg is due to methanol molecules hydrogen bonded to the former. The SDF of the hydroxyl hydrogens shows a high density in the vicinity of the ester and the keto oxygens indicating hydrogen bonding of methanol molecules with these groups. How the arrangement of the two methanol molecules affects the solubility/aggregation of chlorophylls is not clear from the simulations.

The pair correlation function $g_{\text{Mg,C}}$ of carbon atoms of benzene molecules around the Mg has the first peak at 0.35 nm (Figure 7c), which is similar to the distance of 0.38 nm between Mg and benzene in the B3LYP/6-31G** optimized chlorophyllide–benzene complex (Figure 9c). The number of solvent molecules in the first solvation shell (up to 0.5 nm radial distance) is 1.65. As in the case of water and methanol, the Mg is slightly displaced out of the plane of the ring by about 0.013 nm. The displacement of the Mg observed in the B3LYP/6-31G** optimized chlorophyllide–benzene (Figure 9c) complex is 0.006 nm. The oblate doughnut shape densities, which slightly are at an angle to the chlorin plane in the SDF of benzene (see Figure 8c), agree well with the position of the benzene molecule in the QM-

optimized structure of chlorophyllide–benzene complex (see Figure 9c).

Binding Energy and Helmholtz Free Energies of Solvation of the Mg Atom. The binding energies of water and methanol molecules in the chlorophyllide A·L₁ calculated using counterpoise corrected B3LYP/6-31G** method are −43.73 and −45.34 kJ/mol, respectively. QM calculations done by Fredj et al.¹⁸ on a similar model of Chl A gave a similar value of −51.46 kJ/mol, for the binding of water to the Mg. The Helmholtz free energy of binding (ΔF_b) obtained from our calculations is −7.95 and −7.96 kJ/mol in water and methanol, respectively. From the experimentally determined equilibration constant ($K = 56 \text{ l mol}^{-1}$) of dimers and the methanol-coordinated Chl A molecules in CCl₄,¹⁷ a ΔF_b value of −10.04 kJ/mol can be estimated. As we expect that the ΔF_b for the binding of methanol to chlorophyllide a is similar to the one with Chl A, the QM calculated value is in good agreement with the experimental data.

The ΔF_b calculated from the MD simulations using the PMF (Figure 10) of the interaction between the methanol molecules and the Mg is −4.45 kJ/mol, which is lower than the value estimated from the experiment. However, it has been shown from QM calculations that the dielectric constant of the medium decreases the binding of the ligands.¹⁸ Thus taking into account the difference in the dielectric constants of the solvents in the experiment (CCl₄, $\epsilon = 2.24$) and the simulations (pure methanol, $\epsilon \approx 20^{53}$), the lower values of the ΔF_b in the simulation can be considered reasonable.

The ΔF_b of water and benzene to the Mg obtained from MD simulations is −1.92 and −0.24 kJ/mol. Though experimental values are not available for these solvents, the values obtained from our simulation seem reasonable.

Chl A Aggregation. The structures of dimers and multimers obtained from the simulation of 10 Chl A molecules in the water

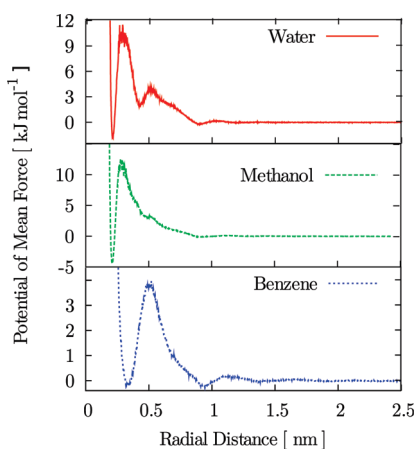


Figure 10. The potential of the mean force of the solvent molecules derived from the radial distribution functions.

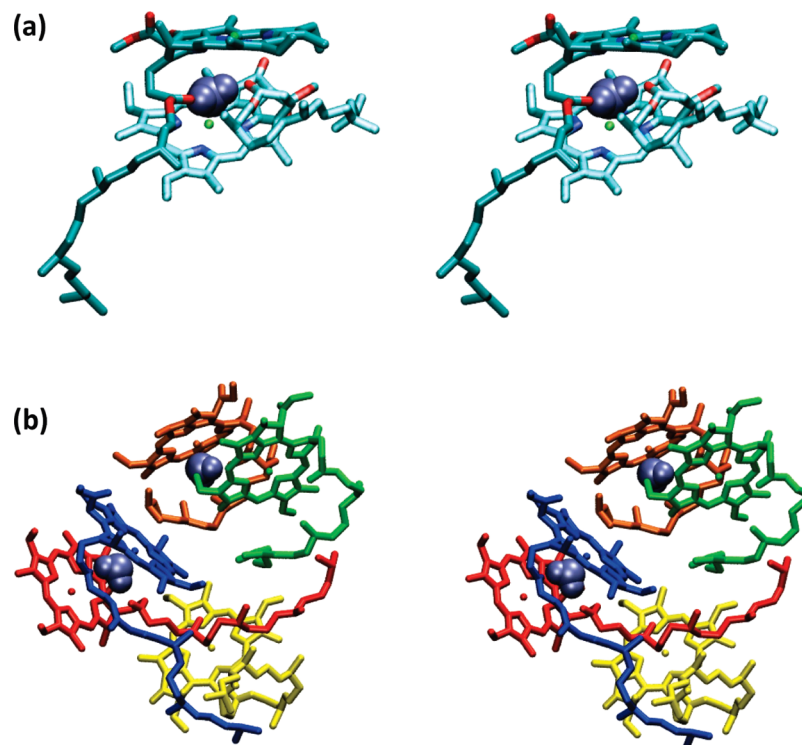


Figure 11. Stereo view of the structures of the dimer (a) and the pentamer (b) of Chl A formed in the water.

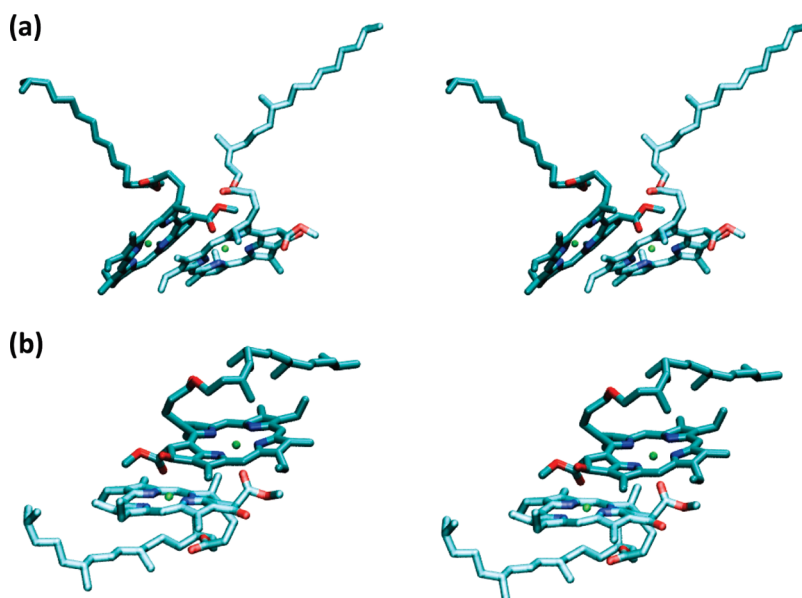


Figure 12. Stereo view of the structures of the dimers of Chl A in the benzene.

and the benzene are shown in the Figures 11 and 12, respectively. No stable dimers or multimers were observed in the simulation in methanol. In the simulation in water, a stable dimer and a pentamer were observed. The spherical shape of the pentamer with the chlorin rings pointing outward is similar to the structure of the large aggregates of Chl A in water-rich regions, as proposed by Agostiano et al.,⁵ wherein the self-aggregation is attributed to the hydrophobic interactions of the phytol tail. The dimer obtained from the water simulation (Figure 11a) has a water molecule sandwiched between the two Chl A molecules, while the pentamer in water (Figure 11b) has two water molecules sandwiched between the Chl A molecules. It is possible that the water molecules trapped in the aggregates also contribute to the aggregation by electrostatic and hydrogen-bonding interactions.

The dimers observed in the simulation in benzene (Figure 12) have different geometries. In the first dimer (Figure 12a), the two molecules are bridged by the binding of the ester C=O group of the first molecule to the Mg of the second molecule. In the second dimer (Figure 12b), the two molecules are bridged by the binding of the ester C=O group of one molecule to the other. Though other dimeric and multimeric conformations are also expected to form,⁵⁴ they probably were not observed in our simulations because of the limited size of the system and the length of the simulations.

Residence Time of Water and Methanol. As reported by Ballschmiter and Katz,⁵¹ a dynamic equilibrium exists between the 2Chl A·L complex and the isolated species for nucleophilic ligand L in nonpolar solvents. The coordination of the ligand to the Mg is primarily responsible for the formation of Chl A·L complex. The time scales of the formation of the complex and its disaggregation can be calculated from the residence time of methanol and water coordinated to the Mg.

In the simulation in methanol, the solvent molecules in close contact to the Mg have residence times spanning from picoseconds up to few nanoseconds. The distribution of the short residence time is shown in Figure 1a of the Supporting Information. The exponential decay approximating the distribution gives a time constant of 5 ps. The distribution of the residence time longer than 100 ps is shown in the panel b of the same figure. The

exponential function fitted to the distribution gives a time constant of 2566 ps.

A similar multi-exponential distribution is observed for the residence times of water molecule in the chlorin ring (see Figure 2 in the Supporting Information). Interestingly, in this case, intermediate time scales (hundreds of ps) are also observed. The three time scales obtained from fitting exponential functions are 10, 200, and 1300 ps, respectively. The shortest and the longest time scales are associated with events involving a fast solvent exchange in the first shell of the Mg caused by molecular collision or conformational change of the chlorin ring. Interaction of other water molecules hydrogen bonded to the Mg-coordinated molecule may be responsible for the presence of the intermediate residence time. However, as there are few data points available for the distributions of the residence times, the calculated decay constants can only be considered qualitatively.

CONCLUSIONS

In this paper, we have presented a new model of chlorophyll a for MD simulations based on the all-atom OPLS force field. The model was tested by studying structural and dynamic properties of the molecule in three different solvents: water, methanol, and benzene. The rotational time constants obtained with our model from the simulations in methanol (125 ps) and benzene (192 ps) are in good agreement with the value extrapolated from experimental data.

The distribution of the phytol tail length in methanol and in benzene is consistent with WLC distribution. The stark differences in the configuration of the tail in different solvents raise interesting questions about the effect of the protein and lipid environment on the distribution of the Chl A in the photosynthetic complex of the chloroplasts. Furthermore, the Mg-coordinating water and methanol molecules have geometries comparable to the available experimental values. In particular, the spatial distribution of the oxygens and hydrogens of water and the methanol molecules support the proposed interaction of these solvent molecules with different functional groups of Chl A. The results of the simulations show that structural and dynamic

properties of the chlorin ring are similar in both methanol and benzene. In methanol and water, the Mg atom in the chlorin ring binds the oxygen of the solvent molecules with residence times of 2566 and 1300 ps, respectively.

The overall good quality of the model makes it suitable for the study of interesting systems like self-assembled micelles,⁵⁵ mimicking the reaction center of light harvesting complexes and interactions of the chlorophylls with inorganic surfaces.

■ ASSOCIATED CONTENT

S Supporting Information. The coordinates of the QM optimized structures of Chl A, chlorophyllide A, complexes of chlorophyllide A with the solvent molecules, the bonded and nonbonded parameters used in the simulations, and the histograms of the residence time of the solvent molecules in the chlorin ring. This information is available free of charge via the Internet at <http://pubs.acs.org/>

■ AUTHOR INFORMATION

Corresponding Author

*E-mail: d.roccatano@jacobs-university.de.

■ ACKNOWLEDGMENT

This study was performed using the computational resources of the Computer Laboratories for Animation, Modeling and Visualization (CLAMV) at Jacobs University Bremen. This work was performed within the graduate program “Nanomolecular Science” and was financially supported by “Research Center for Functional Materials and Nanomolecular Science (NANOFUN)”.

■ REFERENCES

- (1) Katz, J. J.; Oettmeier, W.; Norris, J. R. *Phil. Trans. R. Soc. Lond. B* **1976**, *273*, 227–253.
- (2) Katz, J. J. *Naturwissenschaften* **1973**, *60*, 32–39.
- (3) Agostiano, A.; Cosma, P.; Trotta, M.; Monsu-Scolaro, L.; Micali, N. *J. Phys. Chem. B* **2002**, *106*, 12820–12829.
- (4) Emerson, R.; Arnold, W. *J. Gen. Physiol.* **1931–1932**, *16*, 191–205.
- (5) Agostiano, A.; Monica, M. D.; Palazzo, G.; Trotta, M. *Biophys. Chem.* **1993**, *47*, 193–202.
- (6) Jiao, J.; Thamyongkit, P.; Schmidt, I.; Lindsey, J. S.; Bocian, D. F. *J. Phys. Chem. C* **2007**, *111*, 12693–12704.
- (7) Anariba, F.; Viswanathan, U.; Bocian, D. F.; McCreery, R. L. *Anal. Chem.* **2006**, *78*, 3104–3112.
- (8) Thamyongkit, P.; Yu, L.; Padmaja, K.; Jiao, J.; Bocian, D. F.; Lindsey, J. S. *J. Org. Chem.* **2006**, *71*, 1156–1171.
- (9) Jiao, J.; Anariba, F.; Tiznado, H.; Schmidt, I.; Lindsey, J. S.; Zaera, F.; Bocian, D. F. *J. Am. Chem. Soc.* **2006**, *128*, 6965–6974.
- (10) Zanoni, R.; Aurora, A.; Cattaruzza, F.; Decker, F.; Fastiggi, P.; Menichetti, V.; Tagliatesta, P.; Capodilupo, A.-L.; Lembo, A. *Mater. Sci. Eng., C* **2007**, *27*, 1351–1354.
- (11) Simkiene, I.; Sabataityte, J.; Babonas, G. J.; Reza, A.; Beinoras, J. *Mater. Sci. Eng., C* **2006**, *26*, 1007–1011.
- (12) Linnanto, J.; Korppi-Tommola, J. *Phys. Chem. Chem. Phys.* **2006**, *8*, 663–687.
- (13) Damjanovic, A.; Kosztin, I.; Kleinekathofer, U.; Schulten, K. *Phys. Rev. E: Stat., Nonlinear, Soft Matter Phys.* **2002**, *65*, 1–24.
- (14) Olbrich, C.; Kleinekathofer, U. *J. Phys. Chem. B* **2010**, *114*, 12427–12437.
- (15) Spezia, R.; Aschiy, M.; Nola, A. D.; Valentin, M. D.; Carbonera, D.; Amadei, A. *Biophys. J.* **2003**, *84*, 2805–2813.
- (16) Palencar, P.; Vacha, F.; Kutz, M. *Photosynthetica* **2005**, *43*, 417–420.
- (17) Katz, J. J.; Strain, H. H.; Leussing, D. L.; Dougherty, R. C. *J. Am. Chem. Soc.* **1968**, *90*, 784–791.
- (18) Fredj, A. B.; Ruiz-Lopez, M. F. *J. Phys. Chem. B* **2010**, *114*, 681–687.
- (19) Chow, H.-C.; Serlin, R.; Strouse, C. E. *J. Am. Chem. Soc.* **1975**, *97*, 7230–7237.
- (20) Canc_es, E.; Mennucci, B.; Tomasi, J. *J. Chem. Phys.* **1997**, *107*, 3032–41.
- (21) Mierte_s, S.; Scrocco, E.; Tomasi, J. *Chem. Phys.* **1981**, *55*, 117–129.
- (22) Liu, Z.; Yan, H.; Wang, K.; Kuang, T.; Zhang, J.; Gui, L.; An, X.; Chang, W. *Nature* **2004**, *428*, 287–292.
- (23) Breneman, C. M.; Wiberg, K. B. *J. Comput. Chem.* **1990**, *11*, 361–397.
- (24) Frisch, M. J.; Trucks, G. W.; Schlegel, H. B.; Scuseria, G. E.; Robb, M. A.; Cheeseman, J. R.; Scalmani, G.; Barone, V.; Mennucci, B.; Petersson, G. A.; Nakatsuji, H.; Caricato, M.; Li, X.; Hratchian, H. P.; Izmaylov, A. F.; Bloino, J.; Zheng, G.; Sonnenberg, J. L.; Hada, M.; Ehara, M.; Toyota, K.; Fukuda, R.; Hasegawa, J.; Ishida, M.; Nakajima, T.; Honda, Y.; Kitao, O.; Nakai, H.; Vreven, T.; Montgomery, J. A., Jr.; Peralta, J. E.; Ogliaro, F.; Bearpark, M.; Heyd, J. J.; Brothers, E.; Kudin, K. N.; Staroverov, V. N.; Kobayashi, R.; Normand, J.; Raghavachari, K.; Rendell, A.; Burant, J. C.; Iyengar, S. S.; Tomasi, J.; Cossi, M.; Rega, N.; Millam, J. M.; Klene, M.; Knox, J. E.; Cross, J. B.; Bakken, V.; Adamo, C.; Jaramillo, J.; Gomperts, R.; Stratmann, R. E.; Yazyev, O.; Austin, A. J.; Cammi, R.; Pomelli, C.; Ochterski, J. W.; Martin, R. L.; Morokuma, K.; Zakrzewski, V. G.; Voth, G. A.; Salvador, P.; Dannenberg, J. J.; Dapprich, S.; Daniels, A. D.; Farkas, ;Foresman, J. B.; Ortiz, J. V.; Cioslowski, J.; Fox, D. J. *Gaussian 09*, revision A.1; Gaussian Inc.: Wallingford, CT, 2009.
- (25) Jorgensen, W. L.; Maxwell, D. S.; Tiraldo-Rives, J. *J. Am. Chem. Soc.* **1996**, *118*, 11225–11236.
- (26) Jorgensen, W. L. Chapter OPLS, force field. *Encyclopedia of Computational Chemistry*; Wiley: New York, 1998; Vol. 3, pp 1986–1989.
- (27) Jorgensen, W. L.; McDonald, N. A. *J. Mol. Struct. (THEOCHEM)* **1998**, *424*, 145–155.
- (28) Jorgensen, W. L.; McDonald, N. A. *J. Phys. Chem. B* **1998**, *102*, 8049–8059.
- (29) Jorgensen, W. L.; Chandrasekhar, J.; Madura, J. D.; Impey, R. W.; Klein, M. L. *J. Chem. Phys.* **1983**, *79*, 926–935.
- (30) Milano, G.; Mller-Plathe, F. *J. Phys. Chem. B* **2004**, *108*, 7415–7423.
- (31) Hess, B.; Kutzner, C.; van der Spoel, D.; Lindahl, E. *J. Chem. Theory Comput.* **2008**, *4*, 435–447.
- (32) Hoover, W. G. *Phys. Rev. A: At., Mol., Opt. Phys.* **1985**, *31*, 1695–1697.
- (33) Parrinello, M.; Rahman, A. *J. Appl. Phys.* **1981**, *52*, 7182–7190.
- (34) Nos_e, S.; Klein, M. L. *Mol. Phys.* **1983**, *50*, 1055–1076.
- (35) Miyamoto, S.; Kollman, P. A. *J. Comput. Chem.* **1992**, *13*, 952–962.
- (36) Hess, B.; Bekker, H.; Berendsen, H. J. C.; Fraaije, J. G. E. M. *J. Comput. Chem.* **1997**, *18*, 1463–1472.
- (37) Essmann, U.; Perera, L.; Berkowitz, M. L.; Darden, T.; Lee, H.; Pedersen, L. G. *J. Chem. Phys.* **1995**, *103*, 8577–8592.
- (38) Chandler, D. In *Introduction to modern statistical mechanics*; Oxford University Press: Berkeley, CA, 1987; Chapter 7, page 201.
- (39) Smith, L. J.; Daura, X.; van Gunsteren, W. *Proteins: Struct., Funct., Genet.* **2002**, *48*, 487–496.
- (40) Daura, X.; Jaun, B.; Seebach, D.; van Gunsteren, W. F.; Mark, A. E. *J. Mol. Biol.* **1998**, *280*, 925–932.
- (41) Thirumalai, D.; Ha, B. Statistical Mechanics of Semiexible Chains: A Meanfield Variational Approach. *Theoretical and Mathematical Models in Polymer Research*; Academic Press: San Diego, CA, 1998; pp 1–35.

- (42) Becker, N. B.; Rosa, A.; Everaers, R. *Eur. Phys. J. E: Soft Matter Biol. Phys.* **2010**, *32*, 53–69.
- (43) Allen, M. P.; Tildesley, D. J. *Statistical Mechanics. Computer Simulations of Liquids*; Oxford Science Publications: Oxford, England, 1987; pp 58–60.
- (44) Roccatano, D. *Curr. Protein Pept. Sci.* **2008**, *9*, 407–426.
- (45) Jas, G. S.; Wang, Y.; Pauls, S. W.; Johnson, C. K.; Kuczera, K. *J. Chem. Phys.* **1997**, *107*, 8800–8812.
- (46) Hess, B. *J. Chem. Phys.* **2002**, *116*, 209–217.
- (47) Kulasik, P. G.; Laaksonen, A.; Svishchev, I. M. Spatial Structure in Molecular Liquids. *Molecular dynamics: from classical to quantum methods*; Elsevier Science B.V.: Amsterdam, The Netherlands, 1999; pp 61–90.
- (48) Impey, R. W.; Madden, P. A.; McDonald, I. R. *J. Phys. Chem.* **1983**, *87*, 5071–5083.
- (49) Wiederrecht, G. P.; Svec, W. A.; Niemczyk, M. P.; Wasielewski, M. R. *J. Phys. Chem.* **1995**, *99*, 8918–8926.
- (50) Van Der Spoel, D.; Lindahl, E.; Hess, B.; Groenhof, G.; Mark, A. E.; Berendsen, H. J. *J. Comput. Chem.* **2005**, *26*, 1701–1718.
- (51) Ballschmiter, K.; Katz, J. J. *J. Am. Chem. Soc.* **1969**, *91*, 2661–2677.
- (52) Katz, J. J.; Norris, J. R.; Shipman, L. L.; Thurnauer, M. C. *Annu. Rev. Biophys. Bioeng.* **1978**, *7*, 393–434.
- (53) Richardi, J.; Millot, C.; Fries, P. H. *J. Chem. Phys.* **1999**, *110*, 1138–1147.
- (54) Oba, T.; Furukawa, H.; Wang, Z.-Y.; Nozawa, T.; Mimuro, M.; Tamiaki, H.; Watanabe, T. *J. Phys. Chem. B* **1998**, *102*, 7882–7889.
- (55) Worcester, D. L.; Michalski, T. J.; Katz, J. *Proc. Natl. Acad. Sci. U.S.A.* **1986**, *83*, 3791–3795.